

To appear in the November 2004 issue of the *Astronomical Journal*

Radio-Continuum Emission in Polar-Ring Galaxies

A. L. Cox¹

coxa@beloit.edu

L. S. Sparke²

ABSTRACT

We have used the Very Large Array aperture synthesis telescope to conduct a radio continuum survey of polar-ring galaxies, at 20 cm and 6 cm. Forty objects were observed at 20 cm with $\simeq 5''$ resolution. Twenty (50%) of the program sources were detected at 20 cm, down to our $5\text{-}\sigma$ limit of $0.5 \text{ mJy beam}^{-1}$. This detection rate is similar to those in surveys with comparable sensitivity for early-type galaxies without polar rings. Sixteen of the objects we detected at 20 cm were also observed at 6 cm. We show radio continuum maps for the five objects in our sample that have noticeably extended emission. Our spatial resolution was sufficient to distinguish between emission originating in the host galaxy from that in the polar ring. The radio morphology of the extended sources, as well as the radio to far-infrared flux ratio and the radio spectral indices of our detected sources, indicate that star formation, not nuclear activity, is the dominant source of the radio continuum emission in polar-ring galaxies. However, the implied star-formation rates are modest, and only one of our sample galaxies will consume its supply of cool gas within 500 Myr.

Subject headings: galaxies: elliptical and lenticular, galaxies: interactions, galaxies: peculiar, radio continuum

1. Background & Motivation

Polar ring galaxies (PRG's) are early-type galaxies with rings of gas, stars, and dust that orbit nearly perpendicular to the equatorial plane of the central galaxy. It is generally assumed that they result from an accretion or merger event that occurred some time after the host galaxy formed (Schweizer *et al.* 1983; Whitmore *et al.* 1990, hereafter PRC). Objects that have undergone a

¹ Department of Physics & Astronomy, Beloit College, 700 College Street, Beloit, WI 53511-5595

² Astronomy Department, University of Wisconsin – Madison, 475 N. Charter St., Madison, WI 53706

recent merger often show vigorous star formation (*e.g.*, Schweizer 2000); hence one might expect PRG’s to exhibit signs of enhanced star formation, either in the polar ring or in the host galaxy, as a result of the interaction that formed the polar ring. In many PRG’s, the bulk of the ring material appears to be in regular rotation about the galaxy center (van Gorkom *et al.* 1987; Cox 1996; Arnaboldi *et al.* 1997; Cox *et al.* 2001), and is presumably stabilized in some way. However, some of the accreted ring gas may still be flowing into the host galaxy; high-resolution optical images give indications that this may be happening in NGC 4650A (Gallagher *et al.* 2002). The inflowing gas might fuel an active galactic nucleus (AGN) or cause a burst of star formation in the galaxy center.

Radio continuum emission in galaxies at wavelengths longer than 1 cm is generally dominated by synchrotron radiation from ultrarelativistic electrons. These cosmic rays may be accelerated either by an active nucleus or by supernovae of types Ib or II in star-forming regions. Synchrotron emission from an active nucleus is usually the primary source of radio continuum emission in early-type galaxies (Sadler *et al.* 1989, hereafter SJK89). In star-forming disk systems, the dominant process appears to be acceleration by supernovae (Condon 1992). Radio emission is then cospatial with star formation, and free-free radiation from H II regions will contribute at the higher radio frequencies. It is possible to distinguish between these two mechanisms for accelerating electrons and producing radio continuum flux by examining the radio morphology, the correlation between the radio and far-infrared (FIR) fluxes, and the radio spectral indices of the sources (see Section 4).

Little information is currently available about the radio/FIR correlation or radio spectral indices for PRGs. However, radio continuum emission at 20 cm has been mapped in a few polar rings to date, often in conjunction with observations in the 21 cm line of H I. In the polar ring galaxy ESO 1327-2041 (PRC C-46; Carilli & van Gorkom 1992) about half of the emission comes from the optical center of the galaxy, while the rest is from the brightest knots in the polar ring. In NGC 4650A (PRC A-05; Arnaboldi *et al.* 1997), IC 51 (PRC B-01; Wilkinson *et al.* 1987), and II Zw 71 (PRC B-17; Cox *et al.* 2001), the emission is from the polar material. The implication is that the radio emission in these galaxies is from widespread star formation; it is not dominated by active or star-forming nuclei, perhaps because little of the polar gas is finding its way to the central regions.

We have used the Very Large Array (VLA¹) aperture synthesis telescope to map a sample of PRG’s in the 6 cm and 20 cm bands of radio continuum, to measure the total fluxes, and determine whether the emission comes primarily from the galaxy center or from the polar material. We compare our detection rate and radio spectral indices with those found in radio continuum surveys of early-type galaxies without polar rings (Sadler 1984; Wilkinson *et al.* 1987; Sadler *et al.* 1989; Wrobel 1991a,b). We also examine the morphology, radio/FIR correlation, and radio spectral indices for these galaxies, asking whether the emission is likely to be a consequence of ongoing star

¹The National Radio Astronomy Observatory is a facility of the National Science Foundation operated under cooperative agreement by Associated Universities, Inc.

formation or an AGN. Assuming that star-formation is the dominant source of the radio emission, we derive star-formation rates and gas-consumption timescales for the survey PRGs.

2. Sample Selection & Observations

We have conducted a survey of 40 PRG’s in the 20 cm and 6 cm bands, using the VLA “B” and “C” configurations, respectively, to obtain maps with matched resolution ($\simeq 5''$) in the two bands. The objects in our sample were chosen from categories A, B, or C (confirmed, probable, or possible polar rings) of the “Polar-Ring Catalog” (PRC). We selected those with $\delta \geq -30^\circ$ (far enough north for a good synthesized beam with the VLA) and angular size $\leq 4'$. The latter criterion eliminated NGC 660 (PRC C-13), a known starburst galaxy (van Driel *et al.* 1995), and NGC 3384 (PRC C-34). We also removed the known quasar 3CR 249.1 (PRC C-36) from our sample. Fifty-nine galaxies met these criteria. Forty of these were observed at 20 cm, selected only by the hour angles available at our scheduled observing times. Sixteen of our 20 cm targets were also observed at 6 cm, selecting preferentially those galaxies detected at 20 cm or with known redshifts. The basic data for these galaxies, including positions, redshifts, and FIR fluxes, are listed in Table 1.

Standard calibration and mapping procedures were followed. Maps were made with uniform weighting to maximize spatial resolution. A source was counted as detected if it was (1) extended and at least $3\text{-}\sigma$ above the noise at either wavelength, or (2) a point source at least $5\text{-}\sigma$ above the noise at either wavelength, at the position of the target galaxy. The probability of detecting an unrelated source brighter than 1 mJy within $5''$ of the target galaxy is only 0.05% (White *et al.* 1997) — confusion with background sources should not be a significant problem at these detection limits.

For the most distant objects in our survey, our detection limit would allow us to detect any galaxy with an excess of radio emission (larger than a few times that of a normal spiral galaxy; see Kellermann & Owen (1988)). We detected 20 of the 40 observed galaxies at 20 cm, and 13 of the 16 observed galaxies at 6 cm. Our detection rate of 50% at 20 cm, down to a $5\text{-}\sigma$ limiting flux density of $\simeq 0.5 \text{ mJy beam}^{-1}$, is similar to the 42% detection rate of elliptical galaxies with shells, down to the same limiting flux density, found by W87. These detection rates are not significantly different from the population of “normal” early-type galaxies studied by SJK89 (also 42%) and Wrobel & Heeschen (1991, hereafter WH91).

The radio continuum fluxes and radio spectral indices for our sample are shown in Table 2, along with 21 cm fluxes and H I masses, when available. For non-detections, we show $5\text{-}\sigma_{RMS}$ upper limits, assuming any continuum emission is unresolved. For unresolved sources, the total uncertainty was calculated by adding two terms in quadrature: An assumed 3% uncertainty in the total flux due to calibration σ_{cal} (e. g., Wrobel & Heeschen 1991), and the RMS uncertainty σ_{RMS} measured in the CLEANed images. Typical RMS uncertainties were $0.1 \text{ mJy beam}^{-1}$ at 20 cm and $0.08 \text{ mJy beam}^{-1}$ at 6 cm (with ranges between $0.06\text{-}0.2 \text{ mJy beam}^{-1}$ and $0.03\text{-}0.11 \text{ mJy beam}^{-1}$,

respectively). For extended sources, the RMS uncertainty in the integrated flux is increased by a factor of \sqrt{N} , where N is the number of beam areas over which we integrated to measure the source flux. The total uncertainty is thus the calibration error σ_{cal} , added in quadrature with $\sqrt{N}\sigma_{RMS}$.

3. Source Morphology

In our sample, 15 (75%) of the 20 sources we detected are unresolved at $\simeq 5''$ resolution. Thirteen of these 15 sources are located at the optical center of the galaxy, to within our $5''$ resolution. One of those thirteen sources, PRC C-73, has two point sources at both 20 cm and 6 cm, at the positions of the two brightest peaks at optical wavelengths. The two unresolved sources for which the radio position does not correspond to the optical center of the target galaxy are PRC A-03 (NGC 2685, the “Helix Galaxy”) and PRC C-60 (ESO 464-G31). The radio source in PRC A-03 lies $10''$ from the galaxy center, at a position angle of 58° , within a region of extended $H\alpha$ emission around the nucleus of the galaxy (Eskridge & Pogge 1997). Though the ionized gas in this region does rotate about the minor axis of the host galaxy (Sil’chenko 1998), it is not part of what has traditionally been called the polar ring, which lies at radii beyond $\simeq 35''$ from the galaxy center. The radio emission in PRC C-60 coincides with the optical center of the galaxy MCG–05-50-009, the companion to ESO 464-G31. These two galaxies together make up the galaxy pair that was included in the PRC as a possible polar ring.

The morphology of the extended sources in our sample is quite different than the radio morphology of typical E/S0 galaxies without polar rings. None of the five sources that have extended structure in our $\simeq 5''$ resolution maps show the “core-jet” structure typical of AGN’s. The radio continuum morphologies are consistent with star formation either in the candidate polar ring (PRC B-01 & B-21) or in an extended region of the central galaxy (PRC C-24, C-28, & C-51). Two of the latter sources do have bright peaks at the galaxy center (PRC C-28 & C-51), but the rest of the radio emission in these two galaxies is diffuse and extends throughout the disk of the central object. Radio continuum maps for the five extended sources, as well as for PRC C-73, are discussed in the following subsections.

PRC B-01 (IC 51, Arp 230)

This galaxy is a well-known shell elliptical galaxy, and was included in the sample of shell elliptical galaxies mapped in the radio continuum by W87. It is listed as a candidate polar-ring galaxy in the PRC because it is known to have a fast-rotating disk or annulus of gas, dust, and stars perpendicular to the apparent morphological major axis of the stellar body. Observations in the 21 cm line and $H\alpha$ by D. Schiminovich (1996, private communication) show gas components that rotate about the minor axis of the dust lane/polar ring, but also emission well above the plane of the dust lane. The H I appears to be associated with the outer shells, while the $H\alpha$ emission is in a “fluffy disk” around the dust lane. Because of the interesting morphology of the radio continuum

in this galaxy, we observed it for 30 minutes in each of the VLA B and C configurations. Thus, we have slightly better sensitivity on this source than on the other sources in our sample (see Table 2).

The majority of the radio continuum emission in this galaxy, at both 20 cm and 6 cm, is aligned with the dust lane (the candidate polar ring). However, with our improved sensitivity, we see filaments that extend well above the optical plane of the candidate polar ring; maps made with both uniform and natural weighting, at both wavelengths, are shown in Figure 1. The morphology of this source indicates that current star formation is the most likely source of the radio continuum emission in this galaxy.

PRC B-21 (ESO 603-G21)

The radio continuum emission in our 20 cm and 6 cm observations is only resolved along one direction, coincident with the major axis of the dust lanes observed in the central portions of the candidate polar ring (PRC; see Figure 2). However, the optical extent of the candidate polar ring is $\simeq 50''$ (PRC), while the 20 cm and 6 cm continuum emission we detect has an extent of only $10''$ - $15''$. Arnaboldi *et al.* (1995) find that most of the emission at $2\mu\text{m}$ (K band) comes from a plane close to that of the dust lane. They suggest that this is not a PRG, but a disk galaxy with abnormally heavy dust extinction and a very blue bulge.

PRC C-24 (UGC 4261)

The 20 cm emission in this galaxy does not appear to be aligned with a particular plane; rather, there is a bright central core, surrounded by an apparently smooth and nearly round “halo” of emission. If the extension to the northeast of the majority of the emission is real, it would be interesting, as it lies approximately along the candidate polar ring in this galaxy (PRC; see Figure 3). Although there may be a bright core of emission in the galaxy center, the radio emission does not exhibit the typical “core-jet” morphology of an AGN.

PRC C-28 (NGC 2748)

The emission in this galaxy extends nearly the entire length of the galaxy disk at 20 cm. There is a bright central core, but it contains only $\simeq 5\%$ of the total emission; nearly all of the 20 cm emission comes from the diffuse component in the galaxy disk. None of the emission appears to be associated with the candidate polar ring (see Figure 4); it is probably due to star formation in the disk of the host galaxy.

PRC C-51 (NGC 6286, Arp 293)

The morphology of the 20 cm emission in this galaxy is very similar to that of PRC C-28 – there is a bright central core, surrounded by diffuse emission that extends throughout the disk of the galaxy (see Figure 5). However, the unresolved core component in this object contains $\simeq 35\%$ of the total 20 cm emission in this object. Again, none of the continuum emission we detect appears to be associated with the candidate polar ring. The high 20 cm flux suggests a starburst (see Section 4). The “polar ring” in this galaxy appears to be incomplete, and the optical morphology of the incomplete ring suggests that NGC 6286 is currently interacting with its close companion, NGC 6285 (PRC).

PRC C-73 (A 2358-2604)

These two point sources correspond to the optical positions of the two brightest peaks at optical wavelengths (see Figure 6), which may be two distinct galaxies in the process of merging. This morphology is consistent with the interpretation in the PRC, that the apparent polar ring feature in this candidate PRG is actually tidal debris oriented so that it resembles a polar ring in projection. The difference between a tidal tail that looks like a polar ring, and an actual polar ring, may simply be a matter of the time at which one observes the interaction. Emission from both faint point sources was included in calculations of total radio flux and the radio spectral index for this object (see Table 2).

4. Star Formation vs. Nuclear Activity

As discussed in Section 3, the radio morphology of the extended sources in our sample is consistent with relativistic electrons from recent supernovae as the source of most of the radio continuum emission. To determine whether this is true for most of the galaxies in our sample, we can examine the radio/FIR correlation and the radio spectral indices for the candidate PRGs.

For the 17 galaxies with known fluxes at both 20 cm and $60\mu\text{m}$, we have plotted the radio versus the FIR fluxes in Figure 7a. As discussed in Section 2, it is unlikely that any of the sources we did not detect contain strong radio sources — our failure to detect them at 20 cm is consistent with the FIR/radio correlation for star-forming galaxies. None of the sources in our sample lies significantly outside the envelope of the correlation for star-forming galaxies (from WH91), and most lie well within it. This is not true for early-type galaxies without polar rings; a large fraction of these “normal” galaxies have significant radio excesses over the FIR/radio correlation shown in Figure 7a, pointing to the presence of AGN’s (*e.g.*, Reddy & Yun 2004; WH91). In our sample, all five of the extended sources have most of their radio power in a diffuse component, and none of the detected sources has a significant radio excess.

It is unclear, however, whether this difference between our result and that for non-PRG’s is due to the presence of a polar ring, or to the proportion of elliptical to lenticular galaxies. WH91 find that elliptical galaxies are much more likely to have a radio excess than lenticular galaxies,

and most confirmed polar rings tend to be around lenticular galaxies rather than elliptical galaxies (PRC; van Driel *et al.* 2000). However, the presence of the polar ring makes the central galaxy difficult to classify without detailed study.

The radio spectral indices for the twelve candidate PRG’s detected at both 20 cm and 6 cm are shown as a histogram in Figure 7b. The errors for these calculated spectral indices were calculated using the $5\text{-}\sigma$ uncertainties in the total fluxes with standard formal error calculations, and are shown in Column 9 of Table 2. With two exceptions (PRC A-03 & B-17), all errors are < 0.1 in spectral index.

Taking $S_\nu \propto \nu^\alpha$, Figure 7b shows a slight excess of “steep-spectrum” objects ($\alpha < -0.5$), compared to “flat-spectrum” objects ($\alpha > -0.5$). Steep-spectrum sources of synchrotron emission are optically thin, and generally correspond either to regions of star formation, or the extended radio lobes of an AGN. We see no evidence for extended radio lobes in these PRG’s. Synchrotron emission from the “core” of an active nucleus is often optically thick, so that the source has a flat spectrum. The only one of the flat-spectrum objects that is extended (PRC B-21; see Figure 2) does not have the core-jet morphology typical of an AGN. Thus, no more than four of our sources have the morphology and spectral indices expected if AGN’s contribute significantly to the radio emission.

Assuming, therefore, that all of the 20 cm emission in these galaxies is due to star formation, rather than AGN’s, we have used the formula of Condon (1992) to calculate the rate at which massive ($M > 5 M_\odot$) stars are formed from the radio continuum emission (see Figure 7c). Interestingly, the category “A” and “B” galaxies (confirmed and probable PRG’s; shown as open circles in Figure 7c) have lower star-formation rates, on average, than the category “C” galaxies (possible PRG’s; shown as filled circles in Figure 7c). None of these implied star-formation rates are high, compared to normal disk galaxies. For those galaxies with known H I masses (see Table 2), we use these star-formation rates to compute gas-consumption timescales, assuming a Salpeter initial mass function truncated at $M < 0.4 M_\odot$ (Figure 7d). Only one of the galaxies in our sample, PRC C-51, could use up all of its gas in $\sim 10^8$ years, and thus may fall into the category of “starburst” galaxies. Although the majority of the radio emission in these candidate PRGs likely arises from recent star-formation activity, the rates implied are not high compared to the total available gas in the galaxies.

We conclude that polar-ring galaxies have radio continuum fluxes typical of normal (non-polar-ring) elliptical or S0 galaxies. The morphology of the extended sources, the spectral indices, and FIR fluxes of the PRG’s in our sample indicate that the radio emission is predominantly due to star-forming regions rather than nuclear activity. However, the rate of starbirth is modest — all but one of our sample galaxies have enough cool gas to fuel their star formation for at least another gigayear.

ALC and LSS acknowledge support from the National Science Foundation through grants

AST-9320403 and AST-9803114. The work reported here forms part of the PhD thesis of Andrea Cox, who was an NRAO Predoctoral Fellow while much of it was carried out. ALC would also like to acknowledge Beth Blount (Beloit College '99), who contributed to this paper. The idea for this survey was a suggestion by Peter Biermann at the Max-Planck-Institut für Radioastronomie in Bonn, Germany; we are grateful to Barry Clark for arranging “filler time” at the VLA. This research has made use of the NASA/IPAC Extragalactic Database (NED) which is operated by the Jet Propulsion Laboratory, California Institute of Technology, under contract with the National Aeronautics and Space Administration. Optical images in Figures 1-6 were taken from the Digitized Sky Survey (DSS), produced at the Space Telescope Science Institute under U.S. Government grant NAG W-2166.

REFERENCES

- Arnaboldi, M., Freeman, K. C., Sackett, P. D., Sparke, L. S., & Capaccioli, M. 1995, *Plan. Space Sci.* 43, 1377
- Arnaboldi, M., Oosterloo, T., Combes, F., Freeman, K. C., & Koribalski, B. 1997, *AJ*, 113, 585
- Bottinelli, L., *et al.* 1993, *A&A Supp*, 102, 57
- Carilli, C. L., & van Gorkom, J. H. 1992, *ApJ*, 399, 373
- Condon, J. 1992, *ARA&A*, 30, 575
- Cox, A. L. 1996, *Ph.D. Thesis*, University of Wisconsin-Madison
- Cox, A. L., Sparke, L. S., Watson, A. M., & van Moorsel, G. 2001, *AJ*, 692, 701
- Coziol, R. 1993, *AJ*, 105, 35
- Crawford, T., *et al.* 1996, *ApJ*, 460, 225
- de Vaucouleurs, *et al.* 1991, *Third Reference Catalogue of Bright Galaxies*, version 3.9
- Dressel, L. L., & Condon, J. J. 1976, *ApJ Supp*, 31, 187
- Eskridge, P. B., & Pogge, R. W. 1997, *ApJ*, 486, 259
- Gallagher, J. S., *et al.* 2002, *ApJ*, 568, 199
- Huchra, J., *et al.* 1993, *AJ*, 105, 163
- Kamphuis, J. J., Sijbring, D., & van Albada, T. S. 1996, *A&A Supp*, 116, 15
- Karataeva, G. M., Hagen-Thorn, V. A., & Yakovleva, V. A. 2000, *Ast. Lett.*, 26, 757
- Karataeva, G. M., Yakovleva, V. A., Hagen-Thorn, V. A., & Mikolaichuk, O. V. 2001, *Ast. Lett.*, 27, 74
- Kellermann, K. I., & Owen, F. N. 1988, in *Galactic & Extragalactic Radio Astronomy*, ed. G. L. Verschuur & K. I. Kellermann (New York: Springer Verlag), 563
- Loveday, J. 1996, *MNRAS*, 278, 1025
- Ratcliffe, A., *et al.* 1998, *MNRAS*, 300, 417
- Reddy, N. A., & Yun, M. S. 2004, *ApJ*, 600, 695
- Reshetnikov, V. P., & Combes, F. 1994, *A&A*, 251, 57
- Richter, O.-G., Sackett, P. D., & Sparke, L.S. 1994, *AJ*, 107, 99

- Russell, J. L., *et al.* 1990, *AJ*, 99, 2059
- Sadler, E. M. 1984b, *AJ*, 89, 53
- Sadler, E. M., Jenkins, C. R. & Kotanyi, C. G. 1989, *MNRAS*, 240, 591 (SJK89)
- Schweitzer, F., Whitmore, B. C., & Rubin, V. C. 1983, *AJ*, 88, 909
- Schweizer, F. 2000, *Philosophical Transactions of the Roy. Soc. of London, Series A*, Vol. 358, No. 1772, 2063
- Sil'chenko, O. K. 1998, *A&A*, 330, 412
- van Driel, W., *et al.* 1995, *AJ*, 109, 942
- van Driel, W., Arnaboldi, M., Combes, F., & Sparke, L. S. 2000, *A&A Supp*, 141, 385
- van Gorkom, J. H., Schechter, P. L., & Kristian, J. 1987, *ApJ*, 314, 457
- White, R. L., Becker, R. H., Helfand, D. J., & Gregg, M. D. 1997, *ApJ*, 475, 479
- Whitmore, B. C., Lucas, R. A., McElroy, D.B., Steiman-Cameron, T. Y., Sackett, P. D., & Olling, R. P. 1990, *AJ*, 100, 1489 (PRC)
- Wilkinson, A., *et al.* 1987, *MNRAS*, 224, 895 (W87)
- Wrobel, J. M. 1991, *AJ*, 101, 127
- Wrobel, J. M. 1991, *AJ*, 101, 148
- Wrobel, J. M. & Heeschen, D. S. 1991, *AJ*, 101, 148 (WH91)
- Wunderlich, E., Klein, U., & Wielebinski, R. 1987, *A&A Supp*, 69, 487

Table 1. Observed sources: Data from the Polar-Ring Catalog

Object (PRC)	Alternate Name	Position		Redshift (km s ⁻¹)	60 μ m	100 μ m	Notes
		α_{B1950}	δ_{B1950}		Flux ^a (Jy)	Flux ^a (Jy)	
A-01	A 0136-0801	01 36 26	-08 01 24	5540 ^b	
A-03	NGC 2685, UGC 4666	08 51 40	+58 55 30	876	0.3156	1.6942	“Helix galaxy”
A-04	UGC 7576	12 25 12	+28 58 00	7035 ^b	Banana warp
A-06	UGC 9796, II Zw 73	15 14 00	+43 22 00	5415 ^b	
B-01	Arp 230, IC 51	00 43 53.6 ^c	-13 42 55	1666	2.2144	4.6906	Has shells
B-03	IC 1689	01 20 57	+32 47 28	4567	Confirmed PRG ^d
B-09	UGC 5119	09 34 08.1	+38 19 01	6037 ^e	
B-10	A 0950-2234	09 50 35.2	-22 34 27	14692	
B-11	UGC 5600	10 19 17.2	+78 52 52	2769 ^f	3.4639	4.9607	Inner ring? ^g
B-12	ESO 503-G17	11 24 24	-27 25 48	10313 ^f	
B-16	NGC 5122	13 21 36.8	-10 23 39	2855 ^b	Confirmed PRG ^h
B-17	UGC 9562, II Zw 71	14 49 12	+35 45 00	1255 ^b	Confirmed PRG ^b
B-20	A 2135-2132	21 35 31.1	-21 32 41	
B-21	ESO 603-G21	22 48 40.7 ⁱ	-20 30 47	3180 ^f	1.4535	2.8893	Severely warped
B-24	A 2333-1637	23 33 05	-16 37 14	
C-02	A 0017+2212	00 17 16.7	+22 12 00	
C-03	ESO 474-G26	00 44 40	-24 38 36	16246	0.9131	1.7967	Inner & outer rings?
C-04	A 0051-1323	00 51 00.2	-13 23 04	10876 ^j	
C-05	AM 0051-234	00 51 53.5	-23 49 26	20156	0.4437	1.3828	
C-06	NGC 304	00 53 24	+23 51 00	4991	
C-09	NGC 442	01 12 05	-01 17 48	5629 ^f	0.1893	1.54	
C-12	UGC 1198, VII Zw 3	01 40 58.2	+85 00 38	1149 ^f	2.58	3.22	
C-24	UGC 4261	08 07 40.2	+36 58 38	6446 ^e	1.1426	1.56	
C-25	UGC 4323	08 15 36.3	+67 08 20	4061 ^e	0.1295	(1.1583)	
C-27	UGC 4385	08 21 04.0	+14 54 49	1954 ^f	
C-28	NGC 2748	09 08 02.6 ^k	+76 40 53	1476	7.0358	17.982	
C-29	NGC 2865	09 50 35.2	-22 34 27	14692	

Table 1—Continued

Object (PRC)	Alternate Name	Position		Redshift (km s ⁻¹)	60 μm		100 μm		Notes
		α _{B1950}	δ _{B1950}		Flux ^a	(Jy)	Flux ^a	(Jy)	
C-30	UGC 5101	09 32 05.1	+61 34 33	11945 ^l	11.542		20.226		
C-32	IC 575	09 52 04	−06 37 00	5973 ^m	0.2716		0.9833		
C-35	NGC 3414	10 48 31.8	+28 14 24	1360	0.1907		0.6132		
C-37	UGC 6182	11 05 08.3	+53 53 13	1255		
C-49	NGC 6028	15 59 15.7	+19 29 52	4475		
C-50	UGC 10205	16 04 36	+30 14 00	6605 ^l	0.3939		1.5383		
C-51	NGC 6286, Arp 293	16 57 44.7 ⁿ	+59 00 40	5501 ^e	7.8778		22.595		Interacting; see Fig. 5
C-54	A 2027-2335	20 27 30.8	−23 35 32	...	0.2364		(0.5228)		
C-60	ESO 464-G31	21 15 25.4	−27 33 35	6529 ^f		
C-66	A 2150-1707	21 50 20.9	−17 07 50		
C-69	NGC 7468	23 00 30.5	+16 20 06	2072 ^f	1.2503		1.4890		
C-71	ZGC 2315+03	23 15 42	+03 54 00	18770		Projection effect? ^o
C-73	A 2358-2604	23 58 41.9	−26 04 48	15364 ^p	0.1497		(0.3849)		“Ring” = tidal debris?

^aMost 60 μm & 100 μm fluxes come from the IRAS Faint-Source Catalog (FSC). Fluxes listed to only two decimal places come from the Point-Source Catalog (PSC).

^bCox *et al.* 2001

^cCoziol *et al.* 1993

^dSil’chenko 1998

^eReshetnikov & Combes 1994

^fRichter, Sackett, & Sparke 1994

^gKarataeva *et al.* 2001

^hCox 1996

ⁱoveday 1996

^jHuchra *et al.* 1993

^kDressel & Condon 1976

^lde Vaucouleurs *et al.* 1991

^mBottinelli *et al.* 1993

ⁿRussell *et al.* 1990

^oKarataeva, Hagen-Thorn, & Yakovleva 2000

^pRedshift from Ratcliffe *et al.* 1998

Table 2. Radio fluxes and spectral indices

Object (PRC)	$\int S_{21\text{ cm}} dv^{\text{a}}$ (Jy km s ⁻¹)	M(H I) (10 ⁹ h ⁻² M _⊙)	S _{20 cm} (mJy)	S _{6 cm} (mJy)	$\alpha_{20\text{ cm},6\text{ cm}}$ (S _ν ∝ ν ^α)	Note ^b
A-01	2.2 ^c	1.6	< 0.55	
A-03	34 ^d	0.6	0.70 ± 0.06	0.51 ± 0.08	-0.26 ± 0.21	U
A-04	2.3 ^c	2.7	< 0.55	
A-06	3.7 ^c	2.6	< 0.55	
B-01	~9	~0.6	24.0 ± 0.9	10.7 ± 0.4	-0.67 ± 0.06	E
B-03			< 0.55	
B-09	2.4	2.1	< 0.55	
B-10			< 0.55	
B-11	11	2.0	10.3 ± 0.3	5.5 ± 0.2	-0.52 ± 0.06	U
B-12	1.5	3.8	< 0.55	
B-16	3.4 ^c	0.7	< 0.45 ^c	< 0.55	...	
B-17	6.2 ^e	0.2	1.2 ± 0.20	0.3 ± 0.09	-1.15 ± 0.40	U ^f
			4.5 ± 0.2	1.3 ± 0.1	-1.03 ± 0.11	U
			0.7 ± 0.2	0.9 ± 0.09	+0.21 ± 0.30	U
B-20			< 0.55	
B-21	14 ^g	3.3	9.1 ± 0.5	5.1 ± 0.2	-0.48 ± 0.08	E
B-24			< 0.50	
C-02			< 0.50	
C-03			6.5 ± 0.2	2.5 ± 0.1	-0.79 ± 0.06	U
C-04			0.8 ± 0.08	0.9 ± 0.05	+0.10 ± 0.13	U
C-05			13.4 ± 0.4	4.6 ± 0.2	-0.89 ± 0.05	U
C-06			1.0 ± 0.1	B
C-09	1.5	1.1	< 0.55	< 0.40	...	
C-12	1.0	0.03	4.9 ± 0.2	4.3 ± 0.1	-0.11 ± 0.06	B
C-24	4.6	4.5	11.10 ± 0.4	E ^h
			0.74 ± 0.07	U
C-25	3.6	1.4	1.0 ± 0.1	U
C-27	7.0	0.6	< 0.55	
C-28	30 ⁱ	1.5	38.9 ± 2.0	E
C-29	2.0	10.2	< 0.55	

Table 2—Continued

Object (PRC)	$\int S_{21\text{ cm}} dv^a$ (Jy km s ⁻¹)	M(H I) (10 ⁹ h ⁻² M _⊙)	S _{20 cm} (mJy)	S _{6 cm} (mJy)	$\alpha_{20\text{ cm},6\text{ cm}}$ (S _ν ∝ ν ^α)	Note ^b
C-30 ^j			148.7 ± 0.28	65.4 ± 0.58	-0.68 ± 0.01	B
C-32	1.6	1.3	4.6 ± 0.2	U
C-35	1.0	0.04	3.5 ± 0.1	U
C-37	10	0.4	< 0.50	
C-49	2.0	0.9	< 0.50	
C-50	2.0	2.1	3.6 ± 0.1	U
C-51	1.0	0.7	143 ± 4	E ^k
			9.6 ± 0.4	B
C-54			< 0.55	< 0.45	...	
C-60	5.0	5.0	0.9 ± 0.08	1.1 ± 0.06	+0.17 ± 0.12	U
C-66			< 0.55	
C-69	10	1.0	8.9 ± 0.3	4.1 ± 0.1	-0.64 ± 0.06	B
C-71			< 0.50	
C-73			2.1 ± 0.2	0.56 ± 0.06	-1.10 ± 0.05	U ^l
			2.6 ± 0.1	0.37 ± 0.04	-1.62 ± 0.14	U
			7.8 ± 0.3	2.49 ± 0.1	-0.95 ± 0.07	B

^aUnless otherwise noted, 21 cm line integrals are taken from van Driel *et al.* 2000.

^b“U” means that the source was unresolved in this survey, “B” that it was barely resolved, and “E” that it was extended. All sources were observed with $\simeq 5''$ resolution.

^cCox 1996

^dRichter, Sackett, & Sparke 1994

^eCox *et al.* 2001

^fThe first source is at the position of PRC B-17 (II Zw 71), and the second is at the position of II Zw 70, the interacting companion to PRC B-17. The third source, possibly unrelated, is placed near the eastern extension of the H I gas we observe in PRC B-17 (see Cox *et al.* 2001).

^gPRC B-21 has a close companion with a similar redshift; some of the H I is

probably associated with the companion.

^hThe first source is at the position of PRC C-24 (UGC 4261), and the second source is assumed to be unrelated (see Figure 3).

ⁱKamphuis, Sijbring, & van Albada 1996

^jThe data for this object, including uncertainty estimates, are from Crawford *et al.* (1996).

^kThe first source is at the position of PRC C-51 (NGC 6286), and the second source is at the position of its companion, NGC 6285.

^lTwo faint point sources are observed at the position of PRC C-73 (see Figure 6); the sum of the flux from both of these sources is listed on the first line. The two brighter, more southern sources are probably unrelated.

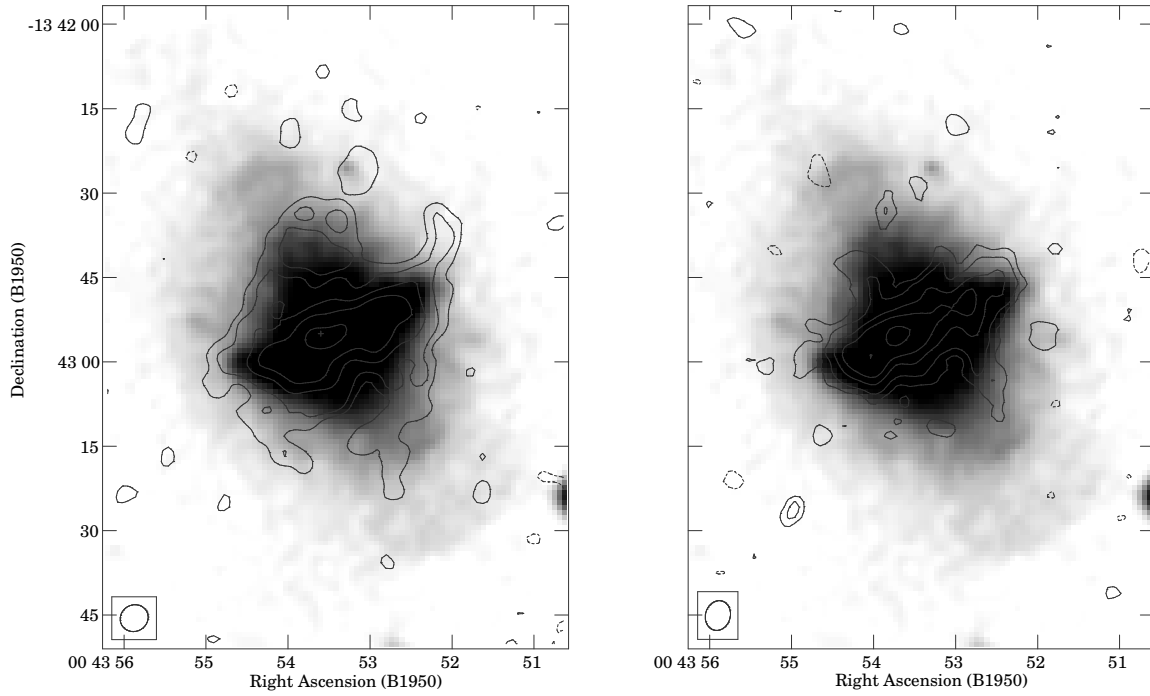


Fig. 1.— Contour plots of the 20 cm (**left**) and 6 cm (**right**) emission in PRC B-01 (IC 51, Arp 230), overlaid on an optical image from the STScI Digitized Sky Survey (DSS). The synthesized beam is shown in the lower right-hand corner. Our $5''$ resolution corresponds to $0.4 h^{-1}$ kpc at the distance of this galaxy. Negative contours are dashed; contours are at $-2.5, 2.5, 4, 7, 10, 15, 20,$ & 25σ ($\sigma=0.07$ mJy beam $^{-1}$ at 20 cm; $\sigma=0.05$ mJy beam $^{-1}$ at 6 cm).

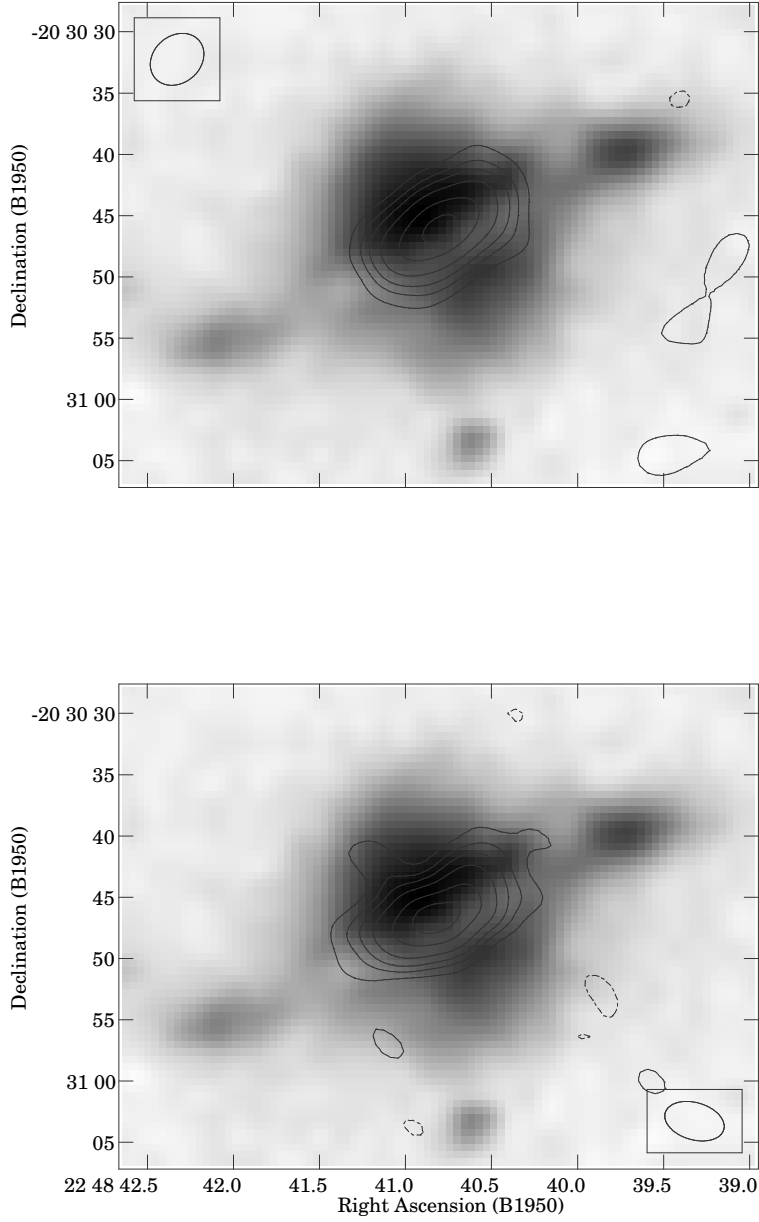


Fig. 2.— Contour plots of the 20 cm (**top**) and 6 cm (**bottom**) emission in PRC B-21 (ESO 603-G21), overlaid on an optical image from the DSS. The synthesized beams are shown in the upper left and lower right corners, respectively. Our $5''$ resolution corresponds to $0.8 h^{-1}$ kpc at the distance of this galaxy. Negative contours are dashed; contours are at $-3, 3, 5, 7, 10, 15, 20,$ & $25\text{-}\sigma$ ($\sigma=0.13$ mJy beam $^{-1}$ at 20 cm; $\sigma=0.05$ mJy beam $^{-1}$ at 6 cm).

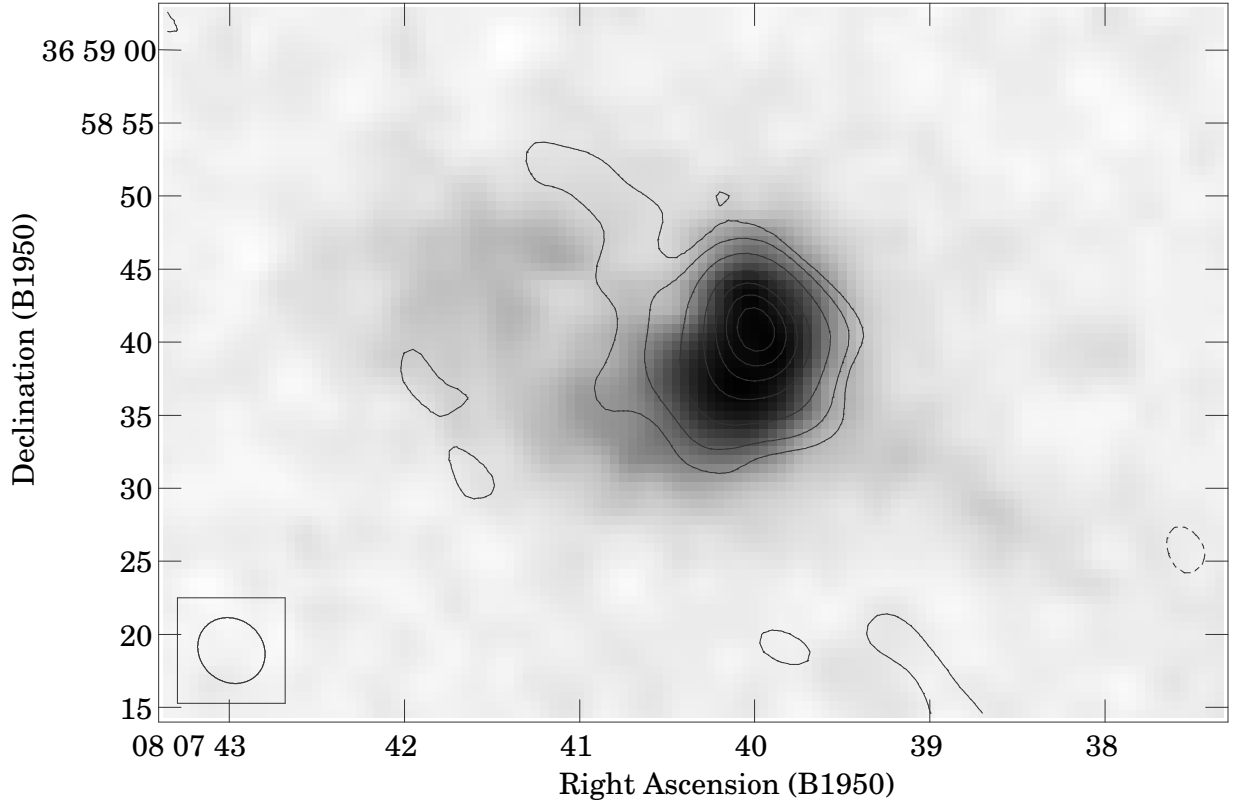


Fig. 3.— Contour plot of the 20 cm emission in PRC C-24 (UGC 4261), overlaid on an optical image from the DSS. The synthesized beam is shown in the lower left corner. Our $5''$ resolution corresponds to $1.6 h^{-1}$ kpc at the distance of this galaxy. Negative contours are dashed; contours are at $-3, 3, 5, 10, 20, 30, 40,$ & $50\text{-}\sigma$ ($\sigma = 0.07 \text{ mJy beam}^{-1}$). The peak flux density at the bright central core is $4.1 \text{ mJy beam}^{-1}$.

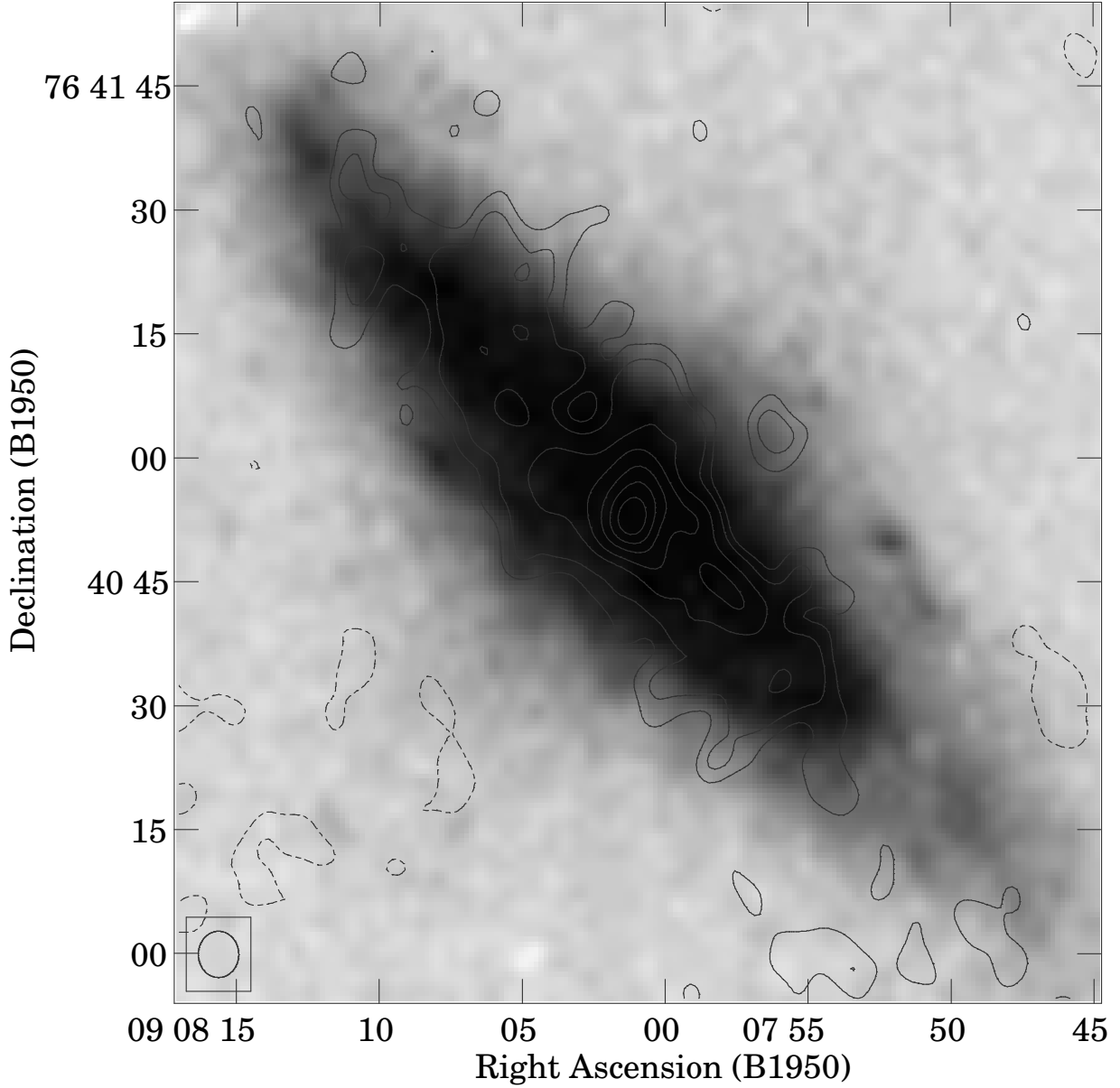


Fig. 4.— Contour plot of the 20 cm emission in PRC C-28 (NGC 2748), overlaid on an optical image from the DSS. The synthesized beam is shown in the lower left corner. Our $5''$ resolution corresponds to $0.4 h^{-1}$ kpc at the distance of this galaxy. Negative contours are dashed; contours are at $-2.5, 2.5, 4, 7, 10, 14, 18,$ & $22\text{-}\sigma$ ($\sigma = 0.10$ mJy beam $^{-1}$).

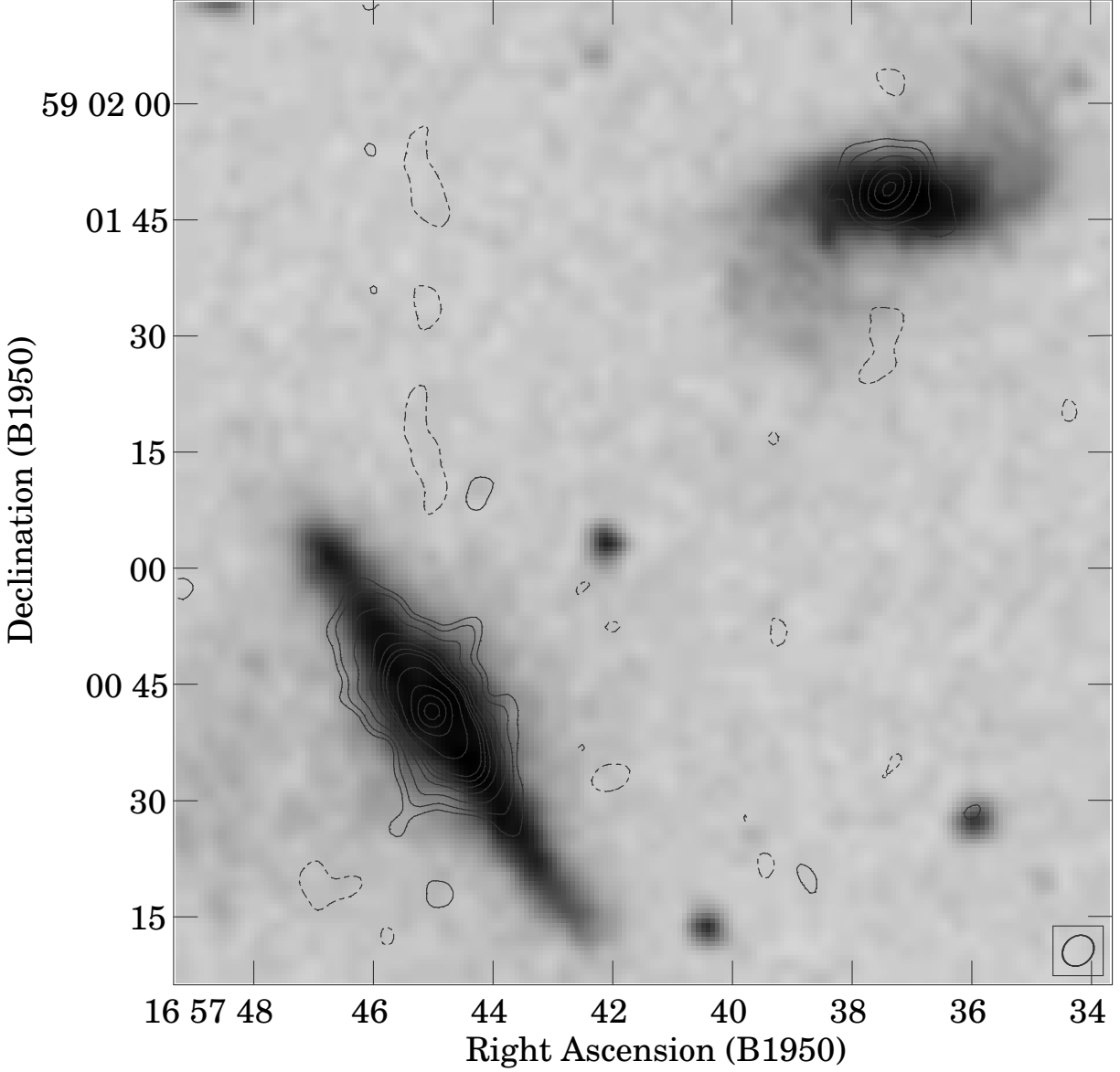


Fig. 5.— Contour plot of the 20 cm emission in PRC C-51 (NGC 6286), overlaid on an optical image from the DSS. The galaxy to the northwest of C-51 is its companion galaxy, NGC 6285. The synthesized beam is shown in the lower right corner. Our $5''$ resolution corresponds to $1.3 h^{-1}$ kpc at the distance of this galaxy. Negative contours are dashed; contours are at $-3, 3, 5, 10, 20, 30, 40, 50, 100, 200, 300, \& 400\text{-}\sigma$ ($\sigma = 0.11 \text{ mJy beam}^{-1}$). The approximately linear negative contours are artefacts of the imaging & deconvolution process.

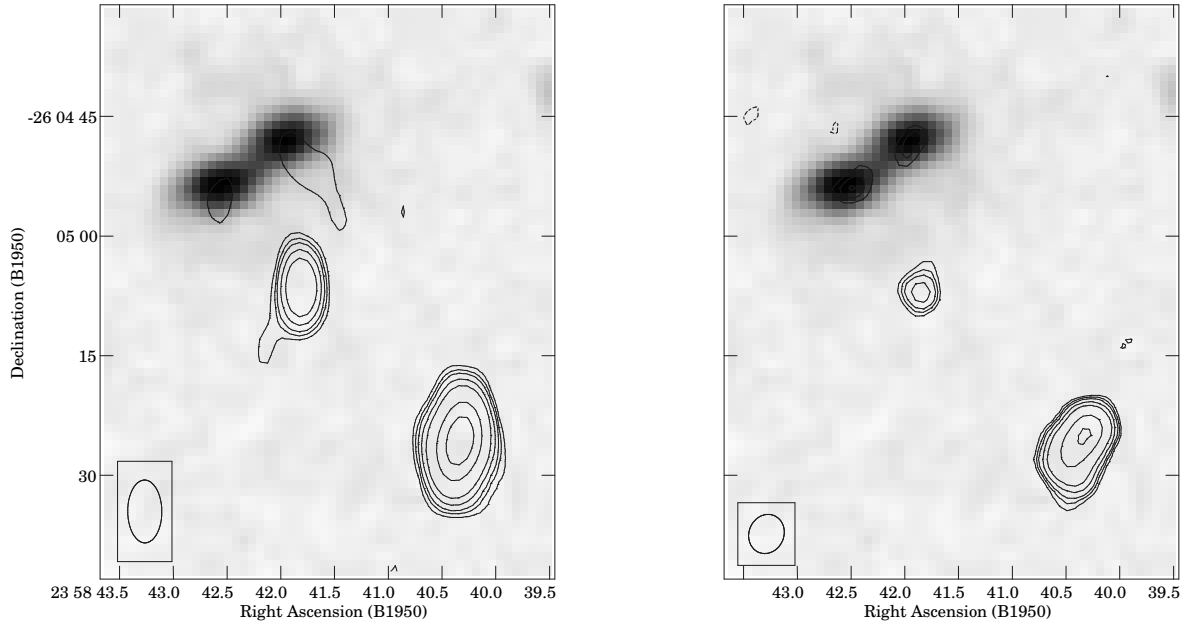


Fig. 6.— Contour plots of the 20 cm (**left**) and 6 cm (**right**) emission in PRC C-73 (A 2358-2604), overlaid on an optical image from the DSS. From both the optical morphology and the presence of two separate radio continuum sources, it is probable that this PRG candidate is a superposition of two (possibly interacting) galaxies. The two brighter continuum sources to the south are probably unrelated. The synthesized beams are shown in the lower left corners. Our $5''$ resolution corresponds to $3.7 h^{-1}$ kpc at the distance of this galaxy. Negative contours are dashed; contours are at $-3, 3, 4, 5, 7, 10, 20,$ & $30\text{-}\sigma$ ($\sigma = 0.11 \text{ mJy beam}^{-1}$ at 20 cm; $\sigma = 0.04 \text{ mJy beam}^{-1}$ at 6 cm).

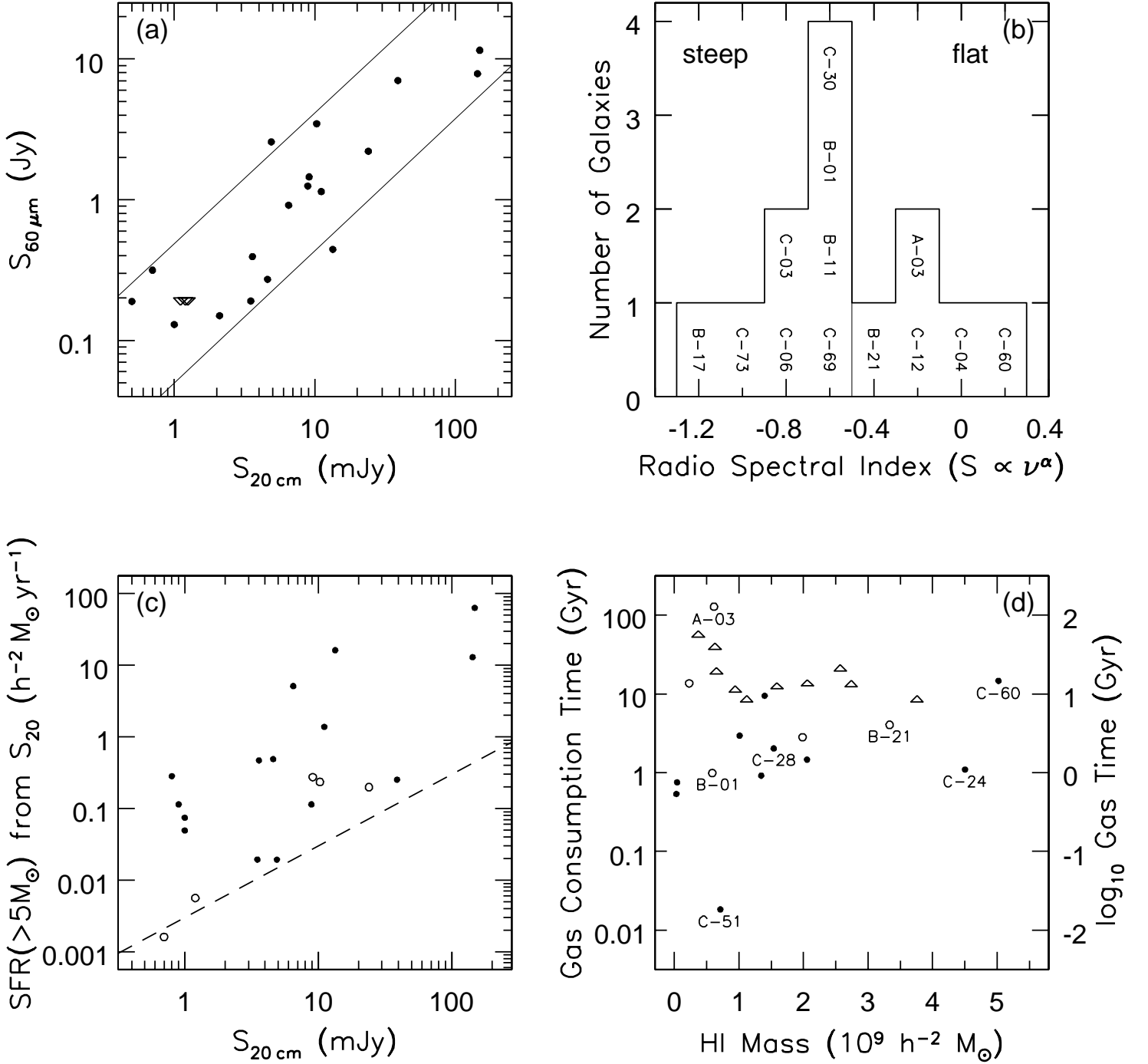


Fig. 7.— (a) 60 μm FIR flux versus 20 cm flux for the galaxies detected in either band. Triangles show upper limits; Sloping lines show the envelope of the FIR/radio correlation for star-forming galaxies from Wrobel & Heeschen (1991), assuming an average radio spectral index $\alpha = -0.5$. (b) Radio spectral indices of detected PRG's at 20 cm & 6 cm. Two of these sources, B-01 & B-21, are extended at $5''$ resolution (see Figures 1 & 2). One of these, C-73, may be two interacting galaxies which look like a PRG in projection (PRC). (c) Birthrate of stars more massive than $5 M_\odot$, calculated from the 20 cm continuum total flux. Category A/B PRG's (open circles) are generally forming stars at a lower rate than category C PRG's (filled circles). The dashed line represents an object at a distance of $10 h^{-1} \text{Mpc}$. (d) H I gas-consumption timescale for PRG's with known 21 cm line integrals (see Table 2). The total SFR is estimated as three times the